Tumor-specific apoptosis caused by deletion of the ERBB3 pseudo-kinase in mouse intestinal epithelium

Daekee Lee,[1,2] Ming Yu,[1,3] Eunjung Lee,[2] Hyunok Kim,[2] Yanan Yang,[4] Kyoungmi Kim,[2] Christina Pannicia,[1] Jonathan M. Kurie,[4] and David W. Threadgill[1,3,5,6]

[1]Department of Genetics, University of North Carolina, Chapel Hill, North Carolina, USA. [2]Division of Life and Pharmaceutical Sciences, Ewha Womans University, Seoul, Republic of Korea. [3]Program in Oral Biology, University of North Carolina, Chapel Hill, North Carolina, USA. [4]Department of Thoracic/Head and Neck Medical Oncology, University of Texas MD Anderson Cancer Center, Houston, Texas, USA. [5]Lineberger Comprehensive Cancer Center, Center for Gastrointestinal Biology and Disease, and Carolina Center for Genome Sciences, University of North Carolina, Chapel Hill, North Carolina, USA. [6]Department of Genetics, North Carolina State University, Raleigh, North Carolina, USA.

Pharmacologic blockade of EGFR or the closely related receptor ERBB2 has modest efficacy against colorectal cancers in the clinic. Although the upregulation of ERBB3, a pseudo-kinase member of the EGFR/ERBB family, is known to contribute to EGFR inhibitor resistance in other cancers, its functions in normal and malignant intestinal epithelium have not been defined. We have shown here that the intestinal epithelium of mice with intestine-specific genetic ablation of *Erbb3* exhibits no cytological abnormalities but does exhibit loss of expression of ERBB4 and sensitivity to intestinal damage. By contrast, intestine-specific *Erbb3* ablation resulted in almost complete absence of intestinal tumors in the *Apc^{Min}* mouse model of colon cancer. Unlike nontransformed epithelium lacking ERBB3, intestinal tumors lacking ERBB3 had reduced PI3K/ AKT signaling, which led to attenuation of tumorigenesis via a tumor-specific increase in caspase-3–mediated apoptosis. Consistent with the mouse data, which suggest that ERBB3-ERBB4 heterodimers contribute to colon cancer survival, experimentally induced loss of ERBB3 in a *KRAS* mutant human colon cancer cell line was associated with loss of ERBB4 expression, and siRNA knockdown of either ERBB3 or ERBB4 resulted in elevated levels of apoptosis. These results indicate that the ERBB3 pseudo-kinase has essential roles in supporting intestinal tumorigenesis and suggest that ERBB3 may be a promising target for the treatment of colorectal cancers.

Introduction

Over the last decade, one of the most pursued molecular targets for colorectal cancer (CRC) treatment has been EGFR, the prototypical receptor tyrosine kinase (RTK) (1). However, with the completion of several clinical trials, it has become increasingly clear that targeting EGFR, either by monoclonal antibody or by small molecule inhibitor, has not resulted in a significant clinical benefit for most patients (2–6). Even dual or pan-ERBB therapeutic approaches, which target EGFR and ERBB2 simultaneously, have achieved limited success against CRCs (7). In this study, we provide strong evidence that ERBB3, a pseudo-kinase member of the ERBB receptor family that lacks a functional kinase, may be a more promising target against CRC.

ERBB3 belongs to the ERBB family of RTKs, which includes EGFR (also known as ERBB1), ERBB2, and ERBB4 (reviewed in ref. 8). Unlike other ERBB receptors, ERBB3 lacks intrinsic kinase activity and cannot autophosphorylate due to the evolutionary acquisition of several changes within the kinase domain (9, 10). Upon ligand binding, ERBB3 can be transactivated on cytoplasmic tyrosine residues by forming heterodimers or higher-order oligomers with other ERBB family members (8). Tyrosine-phosphorylated ERBB3 has the highest binding affinity for PI3K among the ERBB receptors because of 6 YXXM motifs that can directly associate with the p85 regulatory subunit of PI3K (11, 12).

Consequently, activation of ERBB3 frequently results in strong activation of the PI3K/AKT signaling pathway, a critical oncogenic stimulus whose aberrant activity leads to apoptosis resistance in a wide range of cancers (13).

In contrast, the potential for ERBB3 as a target for cancer treatment has been less appreciated due to its defective kinase activity. Nonetheless, accumulating evidence has suggested that ERBB3 plays a critical role in cancer. Overexpression of ERBB3 often accompanies EGFR or ERBB2 overexpression and has been frequently detected in a variety of cancers, including those of the breast (14), colon (15, 16), stomach (17), ovary (18), and pancreas (19). In ERBB2-driven cancers, ERBB3 functions as an intimate signaling partner that promotes the transforming potency of ERBB2, usually by activating the PI3K/AKT pathway (11, 20, 21). ERBB3 is also implicated in coupling EGFR to the PI3K/AKT pathway in non–small cell lung cancers (NSCLCs) that are sensitive to EGFR inhibitors such as gefitinib (22). Conversely, ERBB3-dependent activation of PI3K/AKT by MET leads to acquired resistance to EGFR inhibitors in NSCLCs (23). It is becoming increasingly clear that in cancers driven by EGFR or ERBB2 signaling, ERBB3 functions as a signaling partner to mediate ERBB inhibitor resistance. However, it is not known how ERBB3 supports cancer growth or whether ERBB3 provides essential functions in other cancers such as those of the colon where EGFR and ERBB2 inhibitors have little efficacy. Using an engineered mouse genetic model in vivo and human cell line in vitro, we provide evidence that ERBB3 is essential for CRC growth by preventing apoptosis through ERBB3-ERBB4 heterodimers.

Results

Generation and validation of a conditional Erbb3 allele. Homologous recombination was used to generate an *Erbb3*-null allele (*Erbb3*^tm1Dwt1^) by deletion of exon 2 in order to verify that a conditional allele targeting the same exon would function as a null allele (Figure 1A). Eight targeted ES cell clones were obtained from 194 colonies screened by Southern blot analysis (Supplemental Figure 1A; supplemental material available online with this article; doi:10.1172/JCI36435DS1). The *Neo* selection cassette was removed by transient Cre expression, and colonies with complete excision were identified by PCR. Sequencing of 4 independent PCR-positive clones showed that Cre-mediated excision occurred correctly. One clone with the *Erbb3*^tm1Dwt1^ (also called *Erbb3*^−^) null allele was used to generate chimeric mice that successfully passed the null allele through the germline. The allele was subsequently kept coisogenic on the 129S6/SvEvTAC background or made congenic on a C57BL/6J (B6) background through 10 backcrosses. Intercrosses of heterozygous mice on either background resulted in no *Erbb3*^−^ homozygous mice at 3 weeks of age. Analysis of embryos at 13–15 days post coitum showed that 52% (17 of 33) of *Erbb3*^−^ homozygous embryos were dead, similar to previous analyses of *Erbb3* nullizygous embryos (24, 25), verifying that deletion of exon 2 from *Erbb3* results in a null allele.

To generate the conditional *Erbb3*^tm1Dwt2^ allele (also called *Erbb3*^f^), we used homologous recombination to flank exon 2 with *lox*P sites (Figure 1B). Five targeted ES cell clones were obtained from 242 colonies analyzed by Southern blot analysis (Supplemental Figure 1B). After removing the *Neo* selection cassette in targeted clones by transient expression of Cre, we used one targeted ES cell clone to generate chimeric mice, which successfully transmitted the conditional *Erbb3*^f^ allele through the germline. Intercrossing *Erbb3*^f/+^ with *Erbb3*^+/−^ mice resulted in normal Mendelian ratios of *Erbb3*^f/−^ mice at 3 weeks of age, and these mice were normal and fertile, indicating that the *Erbb3*^f^ allele functions as a wild-type allele (data not shown).

RT-PCR analysis using RNA from the small intestine of *Erbb3*^+/−^ mice resulted in a 517-bp RT-PCR product for the wild-type allele and a 365-bp RT-PCR product for the *Erbb3*^−^ allele due to splicing from exon 1 to 3 creating a nonsense mutation. RT-PCR analysis using RNA from the small intestine of *Erbb3*^f/−^ mice showed the same pattern, indicating that the addition of *lox*P sites does not alter RNA splicing (Supplemental Figure 1, C and D).

The *Erbb3*^f^ allele was verified to function as a null allele after Cre-mediated excision of exon 2 as predicted from the *Erbb3*^−^ allele. Homozygous *Erbb3*-null embryos die at mid-gestation due to defects in the heart, which has underdeveloped endocardial cushions and Schwann cells (23–25). Since developmental defects of nullizygous mutants are known to sometimes occur secondary to placental defects (26), *Erbb3*^+/−^ mice were crossed with *Sox2-Cre*^Tg/+^ mice, which express Cre in epiblast-derived tissues (27). *Erbb3*^+/−^*Sox2-Cre*^Tg/+^ mice were then crossed with *Erbb3*^f/+^ mice and the survival of *Erbb3*^f/−^*Sox2-Cre*^Tg/+^ mice was evaluated. PCR resulted in a 193-bp PCR product specific for the null allele (*Erbb3*^fd^) derived from Cre-mediated excision of exon 2 from *Erbb3*^f^. Among the 50 pups resulting from the cross, none were genotyped as *Erbb3*^f/−^*Sox2-Cre*^Tg/+^ (data not shown). This result demonstrates that embryonic lethality results from loss of *Erbb3* in the embryo proper and also indicates that the *Erbb3*^fd^ allele functions similarly to the *Erbb3*^−^ null allele.

Normal cell proliferation and apoptosis in ERBB3-deficient intestinal epithelium. Semiquantitative RT-PCR analysis comparing relative *Erbb3* mRNA levels across various tissues revealed that relatively high levels of *Erbb3* transcripts are present throughout the gastrointestinal tract, including the stomach, small intestine, and colon (Supplemental Figure 2). To determine whether *Erbb3* is required for normal intestinal homeostasis, we crossed *Erbb3*^f/+^ mice with *Vil-Cre*^Tg/+^ mice, which express Cre throughout the epithelium of the small intestine and colon and in the proximal tubule of the kidneys (28). Mice with intestine-specific deletion of *Erbb3* (*Erbb3*^f/f^*Vil-Cre*^Tg/+^ or *Erbb3*^f/−^*Vil-Cre*^Tg/+^, also called *Erbb3* mutant mice) were compared with control littermates (*Erbb3*^f/+^*Vil-Cre*^Tg/+^, *Erbb3*^+/−^*Vil-Cre*^Tg/+^, or *Erbb3*^f/f^*Vil-Cre*^+/+^). PCR genotyping using ear or epithelial tissues scraped from the surface of the small intestine and colon revealed that the *Erbb3*^fd^ allele was generated only in the small intestine and the colon (Figure 1C). Western blot analysis revealed that ERBB3 expression was completely absent in the epithelial layer of the intestine harvested from *Erbb3* mutant mice (Figure 1D); specific ablation of ERBB3 expression from epithelial cells was verified by immunohistochemistry (Figure 1E and Supplemental Figure 3). Interestingly, alterations in the relative levels of ERBB receptors were observed in the intestinal epithelium of *Erbb3* mutant mice, with slightly higher levels of ERBB2 and almost complete absence of ERBB4. No changes in transcript levels as measured by RT-PCR were observed for any *Erbb* gene, suggesting that deregulated ERBB levels occur posttranscriptionally (data not shown).

To address the effect of intestinal epithelium–specific *Erbb3* deletion on cell proliferation, we compared *Erbb3* mutant mice with controls after BrdU injection. The number of BrdU-positive cells per crypt in the colon was not significantly different between the two groups (Figure 2, A and B). Apoptosis was quantified using the TUNEL assay and also showed no significant alteration in the colons of *Erbb3* mutant mice compared with controls (Figure 2, A and C). The numbers of BrdU- or TUNEL-positive cells was also the same in the small intestine in the two groups (data not shown).

Signaling via PI3K is unique to ERBB3 because of its six p85 subunit binding sites (29, 30). Upon binding of PI3K to ERBB3, phosphatidylinositol-3,4,5-triphophate (PIP$_3$) is produced to recruit signaling molecules containing pleckstrin homology (PH) domains such as the protein serine-threonine kinases AKT1 and PDK1 (31). The relative level of phospho-PDK1 and phospho-AKT1 in intestinal epithelia was similar in *Erbb3* mutant and control mice (Figure 2D). Phospho-RPS6KB1, which is downstream of AKT1, was also expressed at similar levels in intestinal samples from the groups, as was phospho-MAPK1/MAPK3 and phosphorylated stress-induced protein kinase/JNK (phospho-SAPK/JNK). These results show that overall downstream signaling in normal intestinal epithelia is not altered by deletion of *Erbb3*, consistent with a lack of alteration in cell proliferation or cell death.

ERBB3 is required to maintain intestinal homeostasis. The importance of ERBB3 for maintaining intestinal homeostasis in the context of damage was evaluated by measuring susceptibility to intestinal injury caused by dextran sodium sulfate (DSS). Analysis of body weight loss over 8 days of DSS treatment revealed a statistically significant difference between *Erbb3* mutant mice and controls (Figure 3A). After treatment, colon histology was examined. There were statistically significant differences in histological scores between *Erbb3* mutant mice and controls (Figure 3B). Mild lesions revealed loss of mucus cells, glandular hyperplasia, and increased leukocyte levels in the lamina propria. Severe lesions had a complete loss of glandular epithelium, accompanied
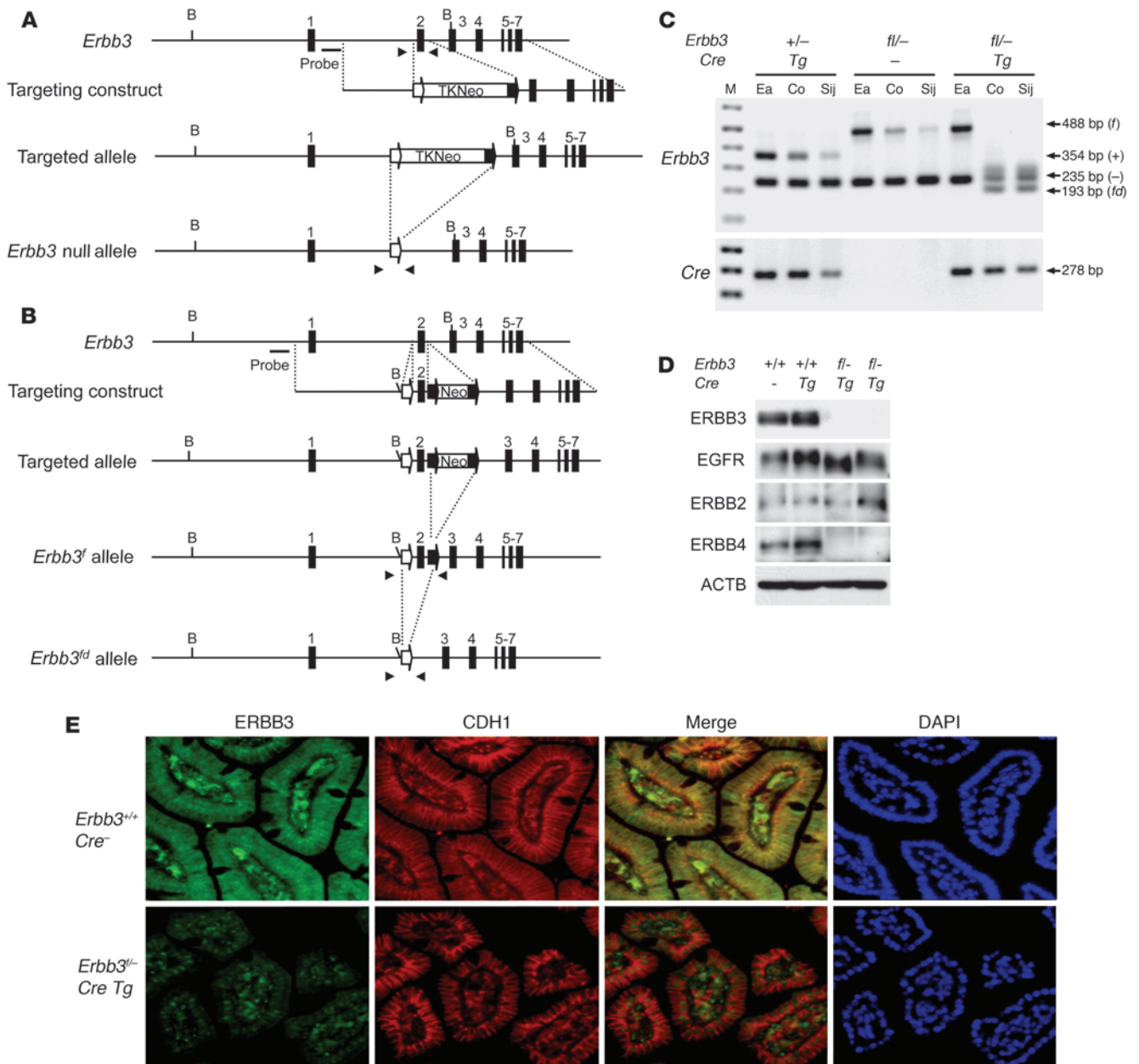
Figure 1

Targeting the *Erbb3* locus. (**A**) Targeted ES cells containing *TK-Neo* flanked by *lox*71 (open symbols) and *lox*P (filled symbols) were transfected with a Cre expression vector to generate the *Erbb3* null allele without exon 2. A fragment upstream of 5′ homology was used as a probe for Southern blots. The primers (arrowheads) were used for PCR to discern the *Erbb3* wild-type and null alleles. (**B**) Targeted ES cells containing exon 2 flanked with *lox*71 and *lox*P were transfected with a Cre expression vector to generate the *Erbb3ᶠ* conditional allele. The *Erbb3ᶠᵈ* allele, generated by Cre-mediated excision of exon 2 in the *Erbb3ᶠ* allele, was induced by breeding with tissue-specific *Cre* transgenic lines. (**C**) PCR genotyping with DNA from ear (Ea), colon (Co), and jejunum (Sij) of *Erbb3ᶠ* mice crossed to *Vil-Cre* mice. Lane M, 1-kb ladder; Tg, *Vil-Cre* transgenic mouse. PCR produces a 488-bp product specific for the *Erbb3ᶠ* allele (*f*), a 354-bp product for the wild-type *Erbb3* allele (+), a 235-bp product for the *Erbb3* null allele (–), a 193-bp product for the *Erbb3ᶠᵈ* allele (*fd*), and a 278-bp product for the *Vil-Cre* transgene. (**D**) Tissue extracts from the epithelium of jejunum analyzed by Western blotting with anti-ERBB3, anti-EGFR, anti-ERBB2, and anti-ERBB4 antibodies. (**E**) Immunofluorescence staining for ERBB3. Representative intestinal sections with wild-type levels of ERBB3 (top) and intestine-specific deletion of ERBB3 (bottom). Staining is shown individually and merged for ERBB3 and the epithelial marker E-cadherin (CDH1). There is background nuclear staining in the ERBB3 mutant tissue. DAPI staining shows locations of nuclei. Original magnification, ×200.
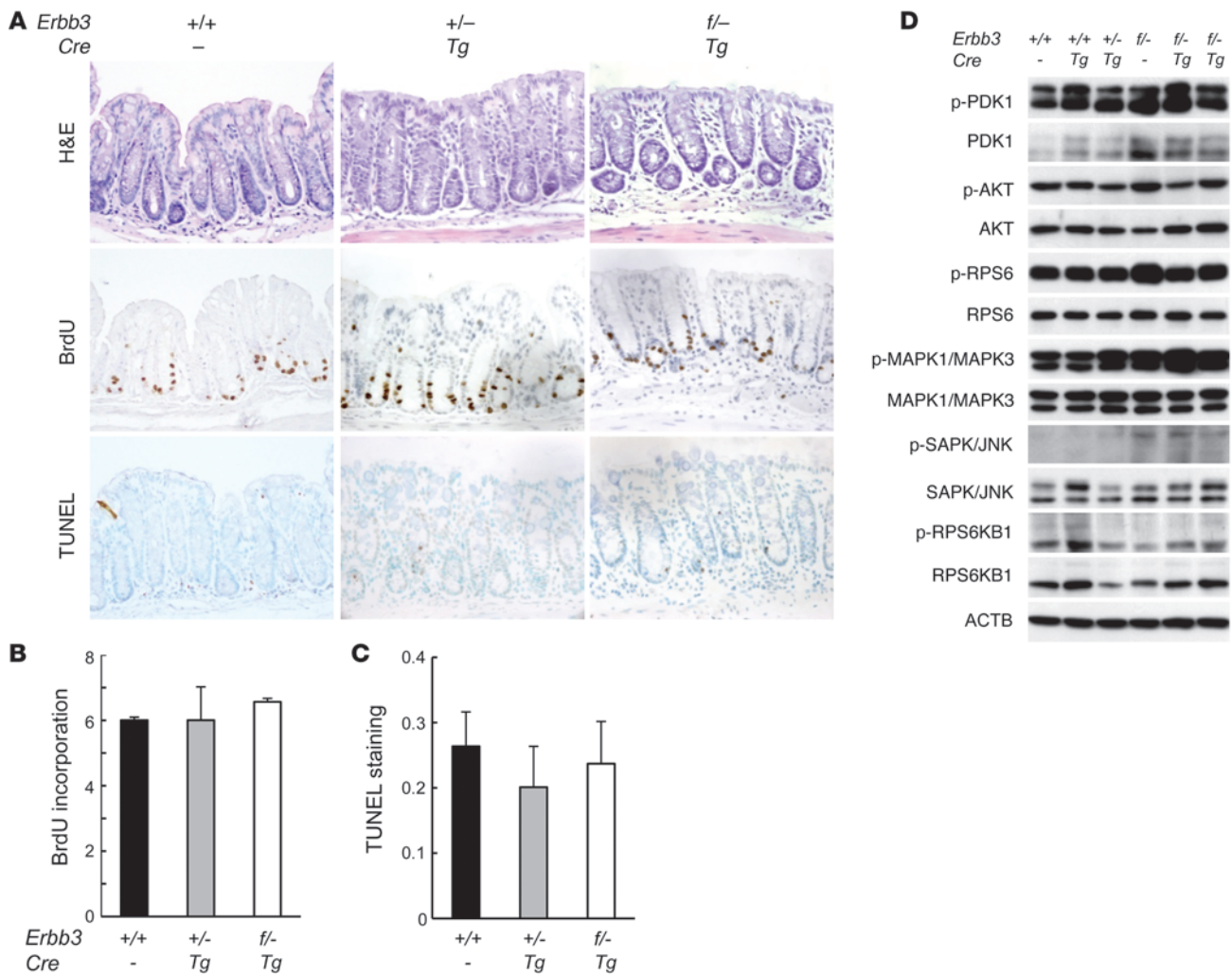
Figure 2
Analysis of intestine-specific *Erbb3*-knockout mice. (**A**) Colon sections from mice injected with BrdU for 2 hours before sacrifice were stained with hematoxylin and eosin Y (H&E), immunostained with anti-BrdU antibody, and assayed for TUNEL-positive cells. Original magnification, ×200. (**B**) Number of BrdU stained cells per crypt in *Erbb3* wild-type, heterozygous *Erbb3*+/−, and *Erbb3* mutant mice. (**C**) Number of TUNEL-positive cells per crypt in wild-type, heterozygous, and *Erbb3* mutant mice. (**D**) Tissue extract prepared from the epithelium of the jejunum from various *Erbb3* genotypes analyzed by Western blotting for the indicated markers. Tg, *Vil-Cre*Tg/+. Error bars indicate SEM.

by collapse of the denuded lamina propria, submucosal edema, fibrinoid necrosis of lamina propria vessels, and infiltration of neutrophils and plasma cells (Figure 3C).

Growth of ApcMin tumors requires ERBB3. Wild-type and *Erbb3* mutant genotypes were combined with *ApcMin* to evaluate the importance of ERBB3 signaling during intestinal tumorigenesis. At 3 months of age, all *ApcMin* mice examined developed visible tumors (>0.3 mm in diameter) in the small intestine regardless of *Erbb3* genotype. However, the number of macroadenomas in the small intestine of *ApcMin*, *Erbb3* mutant mice was reduced dramatically compared with that in *ApcMin* controls (10.6 ± 6.8 vs. 91.9 ± 76.0; Figure 4A). This ERBB3-dependent reduction in the number of small intestine tumors was observed in all regions of the small intestine, with the greatest effect in the duodenum and jejunum (Supplemental Figure 4). Whereas half of the *ApcMin* control mice developed at least 1 colon tumor, no colon tumors were observed in any of the *ApcMin*, *Erbb3* mutant mice (Figure 4B).

Tumors forming in *ApcMin*, *Erbb3* mutant mice, which lack intestinal epithelial expression of ERBB3, were significantly smaller than the tumors that developed in *ApcMin* control mice (size [mean ± SEM, 0.62 ± 0.48 mm vs. 0.94 ± 0.45 mm; Figure 4C), suggesting that ERBB3 signaling is essential for tumor growth. While only 60% of the tumors in age-matched control mice were small, 87.0% of the tumors in *ApcMin*, *Erbb3* mutant mice were less than 1 mm in diameter (Figure 4D). Similarly, the fraction of tumors between 1 and 2 mm in diameter was also reduced in *ApcMin*, *Erbb3* mutant mice compared with controls (9.3% and 38.2%, respectively). Histological analysis of size-matched tumors did not reveal any overt morphological differences related to *Erbb3* genotype (data not shown).

Loss of ERBB3 results in elevated caspase 3–mediated apoptosis in tumors. We measured the level of proliferation and apoptosis within *ApcMin* tumors to determine the cellular mechanism responsible for reduced tumor size in the absence of ERBB3. Immunohistochemical staining with the proliferation marker Ki-67 showed that prolifer-
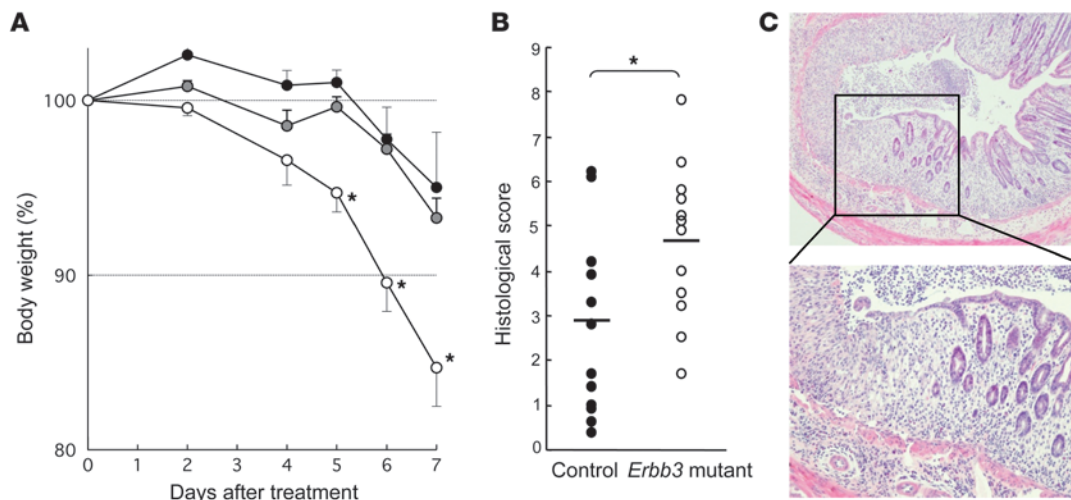
Figure 3
Response of mice with intestine-specific *Erbb3* deletion to DSS treatment. (**A**) Body weights over time expressed as a percentage of the weight on the day of first exposure to DSS. Data are presented as mean ± SD. (**B**) Scoring of histological damage as described in Methods. Each dot represents an individual *Erbb3* wild-type (filled circles), *Erbb3* heterozygous (gray circles) or *Erbb3* mutant (open circles) mouse. Histological scores were significantly different between *Erbb3* mutant and either wild-type or heterozygous mice. Horizontal bars represent means. (**C**) Histological response of colons from *Erbb3* mutant mice to DSS exposure. Top: Low-magnification view (original magnification, ×40) of colon cross section. Bottom: High-magnification view (×200) of inflammation *$P < 0.05$, unpaired Student's *t* test.

ating cells in normal intestinal epithelium are confined to the proliferative zone of the crypts. Irrespective of *Erbb3* genotype, Ki-67–positive cells were expanded in *Apc^{Min}* tumors as identified by colabeling with nuclear CTNNB1 (Figure 5, A–F). The proliferation index, determined by the ratio of Ki-67 to DAPI staining, was not significantly different based on *Erbb3* genotype (Figure 5K). In contrast, apoptosis in tumors measured by TUNEL staining was significantly different based on *Erbb3* genotype (Figure 5, G–J). An increase in the number of TUNEL-positive cells was observed in tumors from *Apc^{Min}*, *Erbb3* mutant mice compared with tumors from *Apc^{Min}* control mice (Figure 5L), showing that loss of ERBB3 leads to elevated cell death via apoptosis specifically in intestinal tumor cells but not in normal intestinal epithelium.

To investigate the molecular mechanism of ERBB3-dependent tumor cell survival, we examined downstream signaling events in individual size-matched tumors from *Apc^{Min}*, *Erbb3* mutant and *Apc^{Min}* control mice (Figure 6A); we analyzed individual tumors from *Apc^{Min}*, *Erbb3* mutant mice to verify lack of ERBB3 expression. The relative phosphorylated/total protein levels of signal mediators downstream of PI3K were lower in tumors from *Apc^{Min}*, *Erbb3* mutant mice compared with *Apc^{Min}* control mice when normalized using ACTB levels to non-tumor epithelium from the same mouse (Figure 6B).

Because there were significant differences in apoptotic indices between control and ERBB3-deficient tumors using the TUNEL assay, individual tumors were analyzed for the relative levels of cleaved caspase-3 (CASP3) and poly(ADP-ribose) polymerase (PARP) (Figure 6A). Total CASP3 levels were decreased in *Apc^{Min}* tumors compared with normal epithelium, as reported previously (32). Consistent with the higher apoptotic index observed in tumors from *Apc^{Min}*, *Erbb3* mutant mice compared with *Apc^{Min}* control mice, the level of cleaved CASP3 was higher in ERBB3-deficient tumors, as was the level of cleaved PARP (Figure 6C).

To validate these results, we performed immunohistochemistry for phospho-RPS6 (Figure 6D). Strong cytoplasmic immunoreactivity

was observed in tumors from *Apc^{Min}* control mice as well as in the nontransformed normal epithelial cells surrounding tumors. However, in size-matched tumors from *Apc^{Min}*, *Erbb3* mutant mice, phospho-RPS6 immunoreactivity was markedly reduced, consistent with the reduced phospho-RPS6 levels observed by Western blot analysis.

Loss of ERBB3 or ERBB4 causes apoptosis in human colon cancer cells. As the disappearance of ERBB4 protein in ERBB3-deficient intestinal epithelium suggests that elevated apoptosis may be due to loss of ERBB3-ERBB4 heterodimers, the dependency on both ERBB3 and ERBB4 was tested using HCT116 human colon cancer cells, a *KRAS* mutant line that is relatively resistant to EGFR inhibition (33). HCT116 cell numbers were significantly attenuated by siRNA knockdown of either ERBB3 (siRNA B3-3) or ERBB4 (siRNA B4-2) (Figure 7A), which was caused by an increase in apoptosis as determined by TUNEL staining (Figure 7, B and C). Although overall cell numbers at the time point measured was not affected by siRNA B3-1, there was a marked increase in cell blebbing compared with controls, which was probably due to apoptosis (Figure 7C). There was no effect on cell numbers or apoptosis using siRNA B4-1 or a scrambled siRNA control.

To determine whether the level of human ERBB4 is dependent on ERBB3 as observed in mice, the expression of all ERBB receptors was analyzed in ERBB3 and ERBB4 siRNA–treated HCT116 cells (Figure 7D). The two siRNAs for ERBB3 showed near complete knockdown of ERBB3 expression. Knockdown of ERBB3 also resulted in a marked reduction in ERBB4 levels similar to that observed in the *Erbb3* mutant mouse intestinal tissue. Only 1 siRNA for ERBB4 (B4-2) reduced ERBB4 levels, which had only a modest effect on ERBB3 expression. No effect was observed on EGFR or ERBB2 after ERBB3 or ERBB4 knockdown. The level of expression of ERBB3 and ERBB4 after siRNA knockdown was consistent with their effects on cell numbers and apoptosis.

The activity of several signal mediators downstream of ERBB3 was also reduced in HCT116 cells treated with ERBB3 or ERBB4
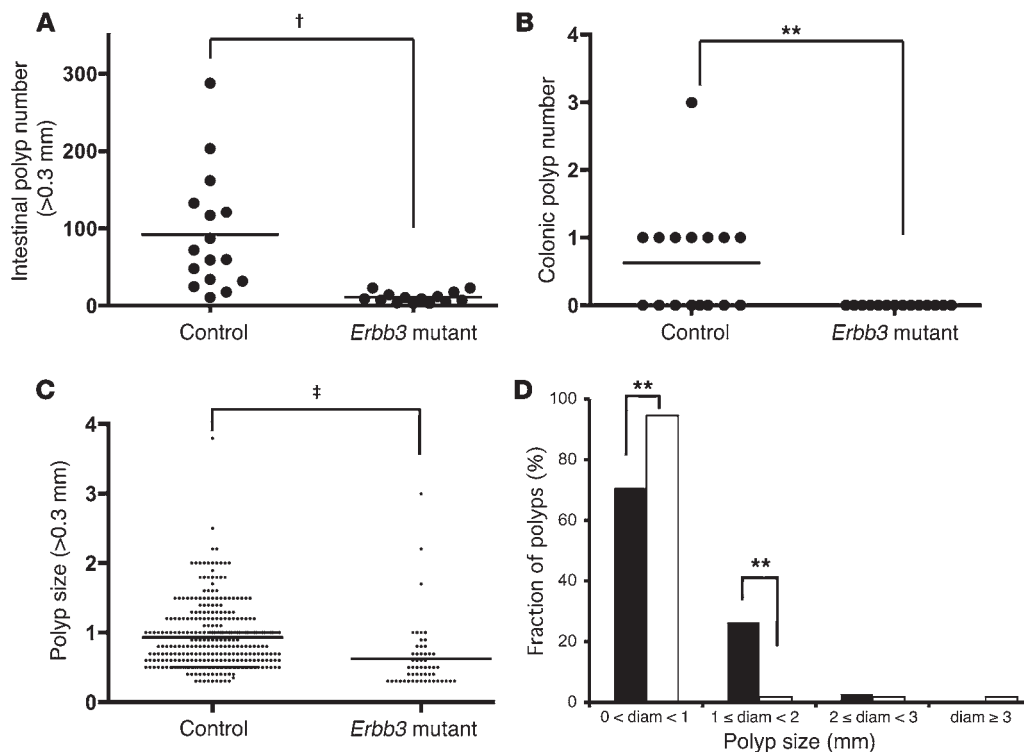
Figure 4
Effect of intestine-specific *Erbb3* deficiency on *Apc^Min* tumor development. (**A**) Intestinal macroadenoma multiplicity in *Apc^Min* mice. Tumor numbers in small intestines of *Apc^Min* mice counted under a dissecting microscope. Each dot represents the total number of tumors (>0.3 mm) from single 3-month-old control (*n* = 16) or *Erbb3* mutant (*n* = 14) mice. Horizontal lines indicate mean tumor number. (**B**) Colonic tumor multiplicity in *Apc^Min* mice. Each dot represents the total number of tumors in the colon from a single mouse. (**C**) Intestinal macroadenoma size analysis. Each dot represents the tumor size of individual tumor. (**D**) Size range of tumors in *Apc^Min* mice. Black bars indicate mean values for *Apc^Min* control mice, and white bars indicate mean values for *Apc^Min Erbb3* mutant mice. †$P < 0.00001$; ‡$P < 0.0005$; **$P < 0.001$; *$P < 0.05$; Wilcoxon rank-sum test. Horizontal bars in **A–C** represent means.

siRNA (Figure 7D). Knockdown of ERBB3 by B3-3 resulted in the largest reduction in phospho-AKT and phospho-RPS6 levels. Cells lines with ERBB3 or ERBB4 knockdown all had elevated PARP cleavage, consistent with elevated apoptosis. Similar to the in vivo results using mice and consistent with the *KRAS* mutant status of HCT116, there was no effect on MAPK activity, which is typically associated with cell proliferation. Overall, these results suggest that ERBB3-ERBB4 heterodimer–dependent AKT pathway activation may be required to prevent colon cancer cell apoptosis.

Discussion
Pseudo-kinases such as ERBB3 are emerging as crucial regulators of diverse cellular functions, despite lacking the ability to directly phosphorylate substrates (34). Using mice with an intestinal epithelium–specific *Erbb3* deletion, we revealed a damage response–specific role for *Erbb3* in intestinal biology. We found that *Erbb3* is not essential for normal intestinal homeostasis, which is supported by normal levels of downstream signal mediators associated with ERBB3. Unlike in normal epithelium, we found that *Erbb3* is essential to protect against intestinal damage caused by chemically induced colitis.

Although ERBB3 lacks intrinsic kinase activity, circumstantial evidence has accumulated suggesting that activation of ERBB3-dependent pathways can modulate cancer phenotypes (17, 35).

Generation of *Erbb3* mutant mice allowed us to examine intestinal tumor development in epithelium deficient for ERBB3 activity. In the *Apc^Min* mouse model, ERBB3 epithelial deficiency has a profound effect on tumor number, reducing it by 90%. Furthermore, there was a complete absence of tumors in the colons of *Apc^Min* lacking epithelial ERBB3. Previous work by our group showed that genetic or biochemical blockade of EGFR activity results in a similarly reduced tumor number in the *Apc^Min* model. However, the residual tumors present in the context of EGFR inhibition are indistinguishable in size from those arising in mice with wild-type *Egfr* (33, 36). Unlike blocking of EGFR signaling, ERBB3 deficiency in mice results in a significant reduction in the average size of the remaining tumors. Our results, albeit more striking, are similar to the concomitant reduction in tumor number and size by treatment with EGFR-related protein (ERRB), which is thought to function as a pan-ERBB inhibitor (37), suggesting that ERBB3 may be the important target for ERRB.

While the extent of proliferation in *Apc^Min* tumors from *Erbb3* mutant mice is comparable to that in animals with wild-type *Erbb3*, a greater number of apoptotic cells was detected in the ERBB3-deficient tumors from *Apc^Min* mice, demonstrating an important role for ERBB3 in tumor cell survival. Strikingly, this was specific to tumors, as normal epithelium remained unaffected. Consistent with a lack of effect on cell proliferation, ERBB3-deficient tumors have normal
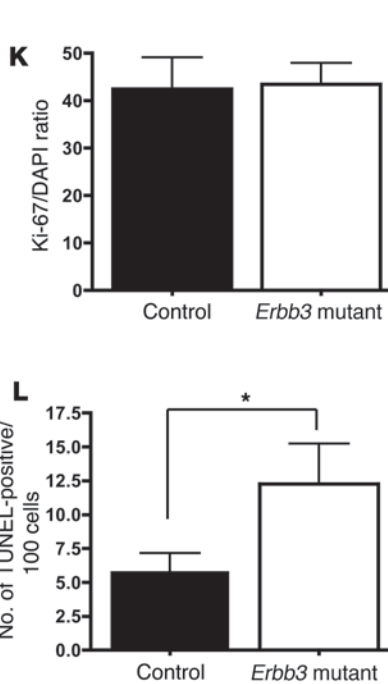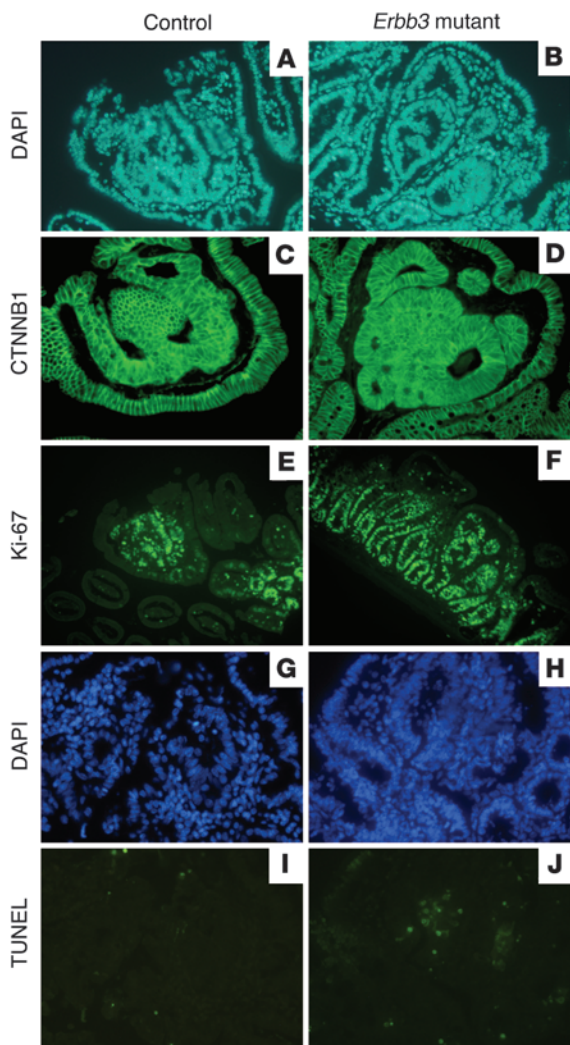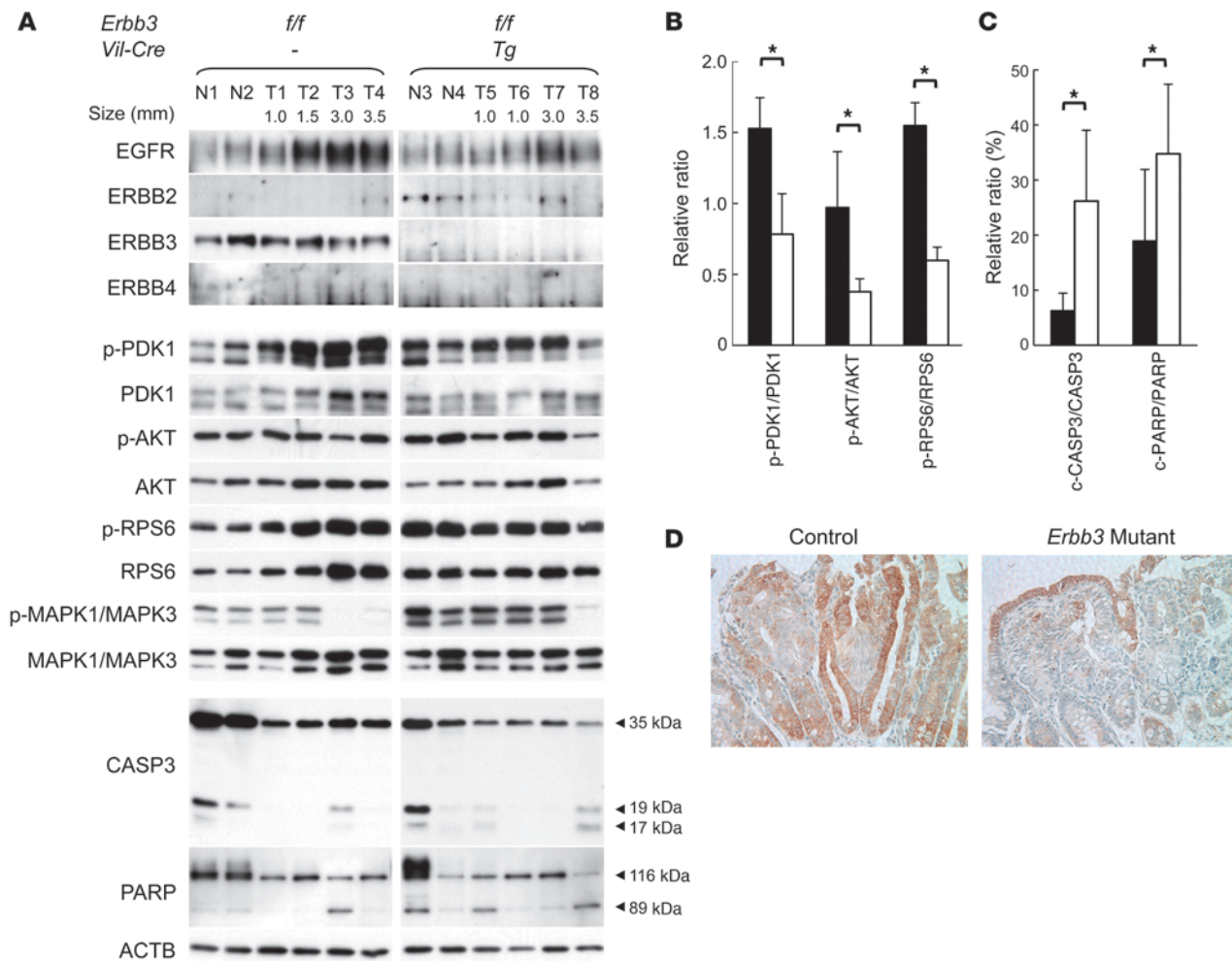
Figure 5
Proliferation and apoptosis in intestinal tumors. (**A** and **B**) DAPI staining, (**C** and **D**) CTNNB1 immunostaining, (**E** and **F**) Ki-67 immunostaining, and (**G** and **H**) DAPI staining with (**I** and **J**) matched TUNEL staining of size-matched intestinal tumors from 3-month-old control ($Apc^{Min}Erbb3^{+/-}Vil\text{-}Cre^{Tg/+}$ and $Apc^{Min}Erbb3^{fl/-}Vil\text{-}Cre^{+/+}$) and $Erbb3$ mutant ($Apc^{Min}Erbb3^{fl/-}Vil\text{-}Cre^{Tg/+}$) mice. Original magnification, ×200. (**K**) Proliferation index as represented by the ratio of Ki-67–positive cells to DAPI-stained cells in Apc^{Min} tumors. (**L**) Graph of apoptosis index as represented by the number of TUNEL-positive cells per 100 cells in tumors. *$P < 0.05$, Student's t test. Error bars represent SEM.

levels of MAPK1/MAPK3 activation, which is the predominant epithelial mitogenic signal. In contrast, the level of phosphorylated RPS6 is significantly reduced in ERBB3-deficient tumors. RPS6 is phosphorylated by RPS6KB1, a major target of FRAP1 (mammalian target of rapamycin [mTOR]) that is downstream of PI3K and AKT. The PI3K/AKT/FRAP1/RPS6 pathway is associated with cell survival through regulation of cell-cycle arrest and apoptosis (38). Considering that numerous growth factors are expressed in the intestinal epithelium, creating redundancy in the activation of RTKs (39), it is surprising that lack of ERBB3 leads to alterations in downstream signaling mediators only upon tumor development.

Our results show that ERBB3 signaling contributes to tumor growth by activating the PI3K/AKT/FRAP1/RPS6 pathway, resulting in prevention of CASP3-mediated apoptosis. Since previous studies showed that genetic or pharmacologic blockade of EGFR leads to a reduction in tumor number but not tumor size (33), we postulate that ERBB3 has a dual role during tumorigenesis (Figure 8). Although we cannot exclude the possibility of essential parallel EGFR and ERBB3 pathways, we propose a model consistent with known ERBB interactions whereby the primary pathway supporting tumor survival in the Apc^{Min} model is through an EGFR-ERBB3 heterodimeric complex that activates both mitogenic and anti-

apoptotic signaling pathways. This complex would be blocked by the absence of either EGFR or ERBB3, which explains the equivalent reduction in tumor number observed in the absence of either receptor. Though EGFR can activate PI3K/AKT through association with the adaptor protein GAB1 in Apc^{Min} tumors (40), our model predicts that activation of PI3K/AKT by EGFR-ERBB3 heterodimers is a major mechanism supporting colon tumor growth. This is consistent with previous studies showing that ERBB3 can couple EGFR to PI3K/AKT (11, 12), leading to an antiapoptotic signal from EGFR.

Our proposed model also predicts that a second pathway, which is EGFR independent but ERBB3 dependent, exists to support survival of a minority of tumors. Cancer survival may be mediated by an ERBB3-ERBB4 heterodimeric complex, since loss of ERBB3 results in a concomitant loss of ERBB4 in both mice and humans and loss of ERBB4 in human colon cancer cells leads to elevated apoptosis. This model is consistent with data showing that with EGFR blockade, the size of remaining tumors in unaffected, while in the absence of ERBB3, the size of remaining tumors is reduced significantly. Loss of EGFR would not affect the secondary pathway, and the tumors arising in the absence of EGFR would not be growth impaired, which is consistent with our previous observations (33).

Figure 6
ERBB3 pathway analysis in *Apc*[Min] tumors. (**A**) Tissue extract from individual tumors and normal epithelia analyzed by Western blotting for ERBB and downstream signal mediators. N, normal epithelium; T, tumors. Signals were quantified by densitometry. (**B**) Normalized ratios (phosphorylated/total) of activities for ERBB3 signal mediators. (**C**) Relative apoptosis levels in each tumor as a function of normal epithelium were determined from the normalized ratios of cleaved to total forms of CASP3 and total PARP. Black bars, mean values for tumors from control mice (*Erbb3*[f/f]; *n* = 4); white bars, mean values for tumors from *Erbb3* mutant mice (*Erbb3*[f/f]*Vil-Cre*[Tg]; *n* = 4). (**D**) Immunostaining for phospho-RPS6 in intestinal tumors from 3-month-old *Apc*[Min], control (*Erbb3*^{+/−}*Vil-Cre*[Tg]) and *Erbb3* mutant (*Erbb3*^{fl/−}*Vil-Cre*[Tg]) mice. Original magnification, ×200. *$P < 0.05$, unpaired Student's *t* test. Error bars represent SEM.

Finally, this model predicts that loss of ERBB3 would not prevent tumors from developing using the secondary pathway. Rather, loss of ERBB3 results in reduced tumor growth rates caused by elevated apoptosis in the absence of efficient PI3K/AKT signaling to RPS6.

The therapeutic implications of these results are that pharmaceutical blockade of ERBB3 may be efficacious against colon cancer. However, there are important differences between pharmaceutical blockade and the genetic ablation reported here, which may result in different responses in the clinic. Genetic blockade results in the loss of ERBB3 and subsequently ERBB4 from the cell surface, while pharmaceutical inhibition of cell surface receptors generally does not result in receptor loss. Rather, pharmaceutical blockade typically inhibits activity of targeted receptors while retaining their expression. If colon cancer survival is dependent upon ERBB4, and expression of ERBB4 is not reduced unless ERBB3 expression is eliminated, then pharmaceutical blockade of ERBB3

may not result in loss of ERBB4 expression. Retention of ERBB4 expression during ERBB3 pharmaceutical blockade may result in a lack of cancer inhibition, in contrast to the present results from genetic studies. This result may be overcome by pharmaceutical blockade of ERBB4.

In this study, we observed a profound ERBB3-dependent reduction in tumor multiplicity and size. The robust tumor-promoting activity of ERBB3 results from its unique link to PI3K/AKT and its downstream effectors FRAP1 and RPS6, leading to inhibition of the proapoptotic mediators CASP3 and PARP. Since kinase-dead ERBB3 must partner with another ERBB to function, lack of ERBB3 would abolish all heterodimers containing ERBB3 simultaneously and abolish efficient signaling to the PI3K/AKT pathway, which may contribute to the pronounced antitumor effects in the absence of ERBB3. Consequently, targeting heterodimeric complexes formed with ERBB3 is predicted to be more efficacious than targeting other
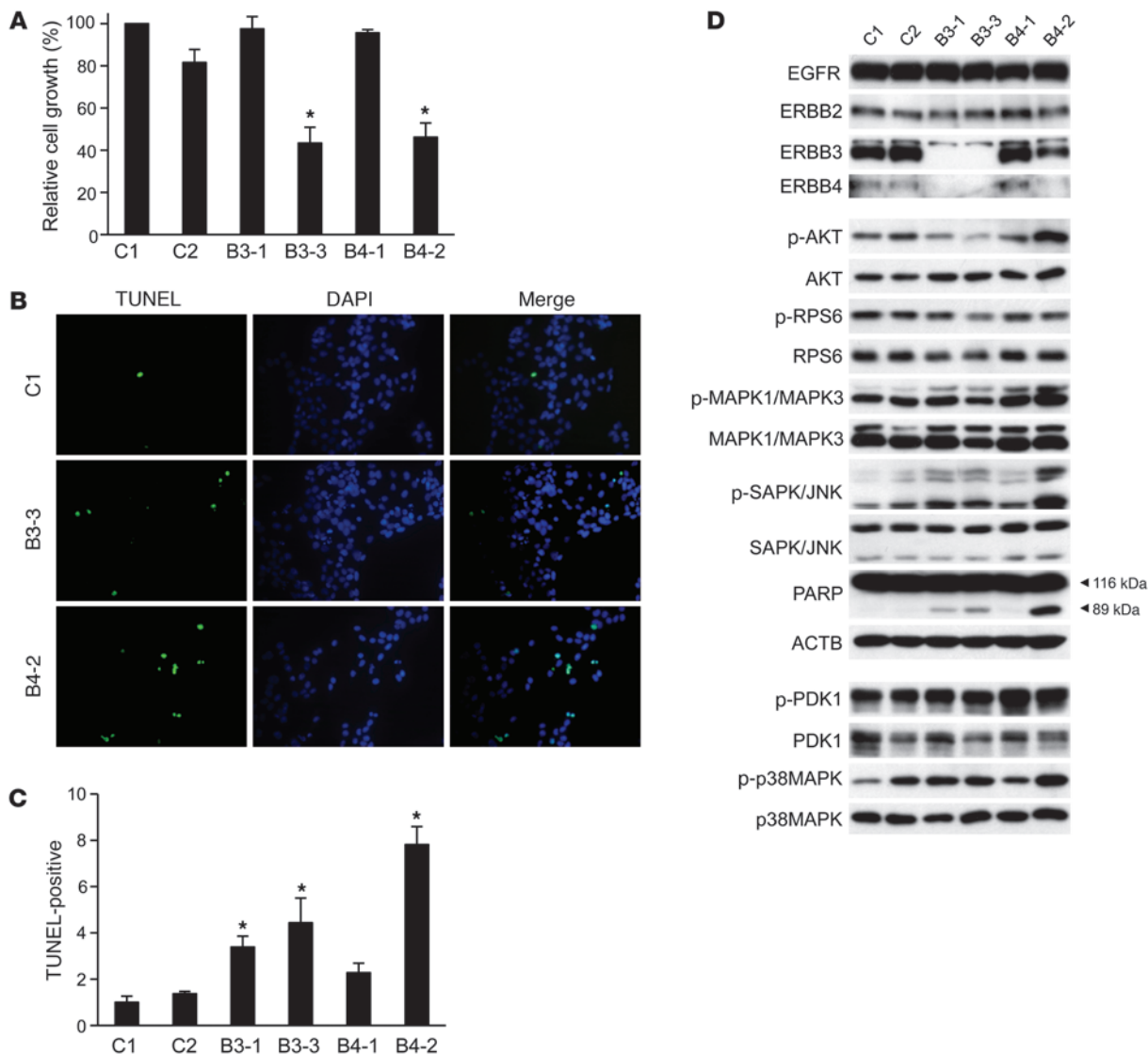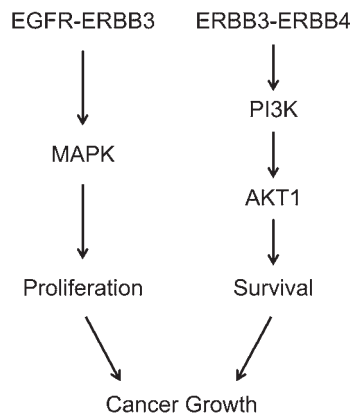
Figure 7
Effect of ERBB3 and ERBB4 knockdown on HCT116 cells. (**A**) Cell proliferation relative to transfection reagent control only. Two negative controls, transfection reagent only (C1) and scrambled siRNA duplex (C2), are shown with ERBB3-siRNA2 (B3-1), ERBB3-siRNA3 (B3-3), ERBB4-siRNA1 (B4-1), and ERBB4-siRNA2 (B4-2). Bars indicate means, with standard errors of 2 independent experiments; each experiment was performed in quadruplicate. *$P < 0.01$, paired Student's t test, 2-tailed compared with C1 or C2. (**B**) TUNEL and DAPI staining after siRNA transfection. Original magnification, ×200. (**C**) Apoptosis index as represented by the percentage of TUNEL-positive cells relative to DAPI-stained cells. More than 400 cells were counted from at least 4 different microscopic fields. Two independent experiments showed similar results. Bars represent mean and SEM. *$P < 0.01$, unpaired Student's t test, 1-tailed compared with C1. (**D**) Western blot of ERBB3 and downstream signal mediators.

ERBB receptors. Our findings also suggest that inhibition of the PI3K/AKT pathway, the major downstream effector of ERBB3-dependent signaling, may be effective in treating intestinal cancers when used in combination with EGFR inhibitors.

Methods

Generation of Erbb3 null allele. Genomic DNA including *Erbb3* was amplified from a GenomeWalker library (Clontech) with sense and antisense primers of exon 2 based on a partial *Erbb3* cDNA sequence of extracellular domain (GenBank accession number AF059175). The resulting genomic DNA fragments of upstream (2.2 kb from a *Pvu*II GenomeWalker library) and downstream (3.6 kb from a *Dra*I GenomeWalker library) of exon 2

were confirmed by sequencing. To construct the targeting vector, a TK-Neo fusion cassette, pTNFUS69Py (41), was flanked with *lox*71 and *lox*P before PCR amplification of the 5′ homology region (2 kb) and 3′ homology region (3.5 kb) using 129S6/SvEvTAC genomic DNA and subcloning the floxed TK-Neo fusion cassette (Figure 1A). Homologous recombination in TL-1 ES cells was performed as described previously (42). Clones were screened for accurate homologous recombination by Southern blot hybridization using DNA isolated from ES cell clones that was digested with *Bam*HI, electrophoretically separated on 0.8% agarose gel, and transferred to a Nylon membrane (Schleicher & Schuell). The membrane was screened with an 0.6-kb probe derived from an *Eco*RV and *Pvu*II DNA fragment upstream of the 5′ homology region. To remove the TK-Neo cassette

EGFR-ERBB3   ERBB3-ERBB4

↓   ↓

              PI3K

MAPK

↓   ↓

              AKT1

Proliferation   Survival

↘   ↙

Cancer Growth

Figure 8
Model of ERBB interactions in colon cancer growth. Data suggest that 2 ERBB-mediated pathways support colon cancer growth. An EGFR-ERBB3-mediated pathway is proposed to be required for tumorigenesis, while an independent ERBB3-mediated pathway is proposed to support cell survival by preventing apoptosis.

in the targeted allele, the targeted ES cell were electroporated with 10 μg pCreEGFP that expresses a Cre-EGFP fusion protein under the human cytomegalovirus immediate early promoter. ES cells were passed once, two days after electroporation, and individual ES cell clones picked at two days after passaging. DNA isolated from ES cell clones was digested with *Bam*HI and analyzed by Southern blotting as described above. Since the *Bam*HI fragment of the endogenous and excised alleles was similar in size by Southern blot analysis, PCR was performed with mErbb3-S1, 5′-TCCAGCGTGGAAAAGTTCAC-3′ and mErbb3-AS1, 5′-AAGCCTTCTC-TATGGAAAGTG-3′ primers. PCR products were subcloned to TOPO2.1 vector (Invitrogen), and Cre-mediated excision was further confirmed by sequencing. Chimeric mice were generated by morula aggregation with CD-1–derived morulas before implantation into surrogate dams (42). Selected chimeras were bred to identify germline transmission of the targeted allele. Subsequent generations of mice carrying the *Erbb3* null allele were maintained isogenic on 129S6/SvEvTAC and, after 10 generations of backcrossing, congenic on B6 genetic backgrounds. Genotypes were determined by PCR with mErbb3-S1 and mErbb3-AS1 primers.

Generation of Erbb3 conditional allele. An *Eco*RV and *Pvu*II fragment upstream of the 5′ homology region of the *Erbb3* targeting vector described above was used as a probe to screen a 129S6/SvEvTAC BAC library (RPCI-22; Roswell Park Cancer Institute). Genomic DNA from one BAC clone, 65B22, was amplified with PCR to generate 5′ homology (3.9-kb) and 3′ homology (3.5-kb) regions, and a fragment containing exon 2 flanked *lox*71 sites. All 3 fragments were inserted into a Pgk-Neo cassette flanked by *lox*P sites to generate the conditional targeting vector (Figure 1B). All ligation junctions were verified by DNA sequencing. Gene targeting was done as described above. DNA isolated from ES cell clones was screened with an 0.65-kb probe derived from an *Eco*RI-to-*Pvu*II genomic DNA fragment upstream of the 5′ homologous arm of the targeting construct. After removal of the Pgk-Neo cassette in the targeted allele as described above, the floxed allele was further screened by PCR with mErbb3-S1 and mErbb3-AS1. Chimeric mice were generated by morula aggregation with CD-1–derived morula and implanted into surrogate dams (42). Selected chimeras were bred to identify germline transmission of the *Erbb3^f* allele. Subsequent generations of isogenic mice carrying the *Erbb3^f* allele were maintained on the 129S6/SvEvTAC background. Genotypes of individual mice were determined by PCR with mErbb3-S1 and mErbb3-AS1 primers.

Mice and crosses. Cre transgenic mice, B6;D2-Tg(Vil-Cre)20Syr (Mouse Models of Human Cancers Consortium, strain number 01XE7) and Tg(Sox2-Cre)1Amc/J, were obtained from NCI-Frederick and The Jackson Laboratory, respectively, and maintained on a B6 background. B6-*Apc^Min* mice were obtained from The Jackson Laboratory. *Erbb3^f/−* mice were crossed to *Cre* transgenic lines to get *Erbb3^+/−Cre^Tg* or *Erbb3^f/+Cre^Tg* mice. These mice were further backcrossed to *Erbb3^+/−* or *Erbb3^f/+* mice to get conditionally targeted *Erbb3* mice (*Erbb3^f/−Cre^Tg* or *Erbb3^f/fCre^Tg*). Although most experiments used *Erbb3^f/−* rather than *Erbb3^f/f* mice to enhance the likelihood of generating cells efficient for ERBB3 upon Cre-mediated excision, no detectable differences were observed between *Erbb3^f/f* and *Erbb3^f/−* mice. All controls were littermates of various genotypes with normal ERBB3 levels. The genotype of each mouse was determined by PCR using mErbb3-S1 and mErbb3-AS1; these primers give a 354-bp product for the wild-type *Erbb3* allele, a 235-bp product for the *Erbb3^−* null allele, a 488-bp product for the *Erbb3^f* conditional allele, and 193-bp PCR product specific for the *Erbb3^fd* Cre-deleted allele. *Cre* transgenic mice were identified using PCR with cre-S1, 5′-GTGATGAGGTTCGCAAGAAC-3′ and cre-AS1, 5′-AGCATTGCTGTCACTTGGTC-3′ primers, which produces a 278-bp PCR product. Mice were genotyped for the *Apc^Min* allele as previously described (33). Mice were fed Purina Mills Lab Diet 5058 under specific pathogen–free conditions in an American Association for the Accreditation of Lab Animal Care–approved facility. Mice were euthanized by CO_2 asphyxiation for tissue collection.

Approval of animal experiments. All experiments involving mice were reviewed and approved by the Institutional Animal Care and Use Committee of the University of North Carolina, Chapel Hill.

BrdU and TUNEL staining. Tissues were labeled with BrdU (Sigma-Aldrich) for 2 hours after intraperitoneal injection with 10 mM BrdU in PBS, pH 7.4, at 0.1 ml/10 g body weight. Small intestines and colons were fixed in 10% neutral buffered formalin (NBF) and embedded with paraffin. Paraffin sections (7 μm) were immunostained with a BrdU staining kit (Zymed, Invitrogen) or with a TUNEL staining kit (Chemicon) according to manufacturer's protocols.

DSS treatment and histological scoring. DSS (36–50 kDa; MP Biomedicals) was dissolved in deionized water at 1.5% (w/v) and administered to mice ad libitum in drinking water. The body weight of each mouse was measured daily. The colon was excised at 8 days after treatment, fixed in 10% NBF, and embedded with paraffin. Paraffin sections (7 μm) were stained with H&E for histological analysis. The severity of mucosal injury was graded on a scale of 0 to 3 as previously described, with minor modifications: grade 0, normal; grade 1, partial destruction of crypts; grade 2, complete loss of crypts; and grade 3, complete loss of crypts and epithelial cells (43). The histological score was determined by multiplying the portion of injured surface by the grade of severity. Three different regions of distal colon were used for histological scoring, and the histological scores from individual mice were determined by adding all 3 values. Histological scoring was performed in a blinded fashion.

Macroadenoma counts. The small intestine and colon were removed from each mouse. The small intestine was cut into thirds, and each segment gently flushed with PBS to remove fecal material, cut longitudinally, and splayed flat. Tumor numbers and diameters were obtained for all tumors with a dissecting microscope and in-scope micrometer. The smallest tumors that can be counted are approximately 0.3 mm in diameter. Tumor scoring was performed by a researcher blinded to genotype. Tumor location along the gastrointestinal tract was also recorded.

Histology and immunohistochemistry. Intestinal tissues or colon samples were rolled into a jelly roll before being fixed in 10% NBF. The processed tissues were embedded in paraffin and sectioned (7 μm). Every 50 μm, sections were taken and stained with H&E. Immunohistochemical procedures

were performed as described previously (44). Intestinal tumors were rapidly dissected, fixed in 10% NBF, and embedded in paraffin before being cut in 7-μm-thick sections. For immunohistology, antigen retrieval was performed by boiling for 20 minutes in citrate buffer, pH 6.0. Sections were treated with 0.3% hydrogen peroxide in PBS for 30 minutes, washed in PBS, blocked in PBS plus 3% goat serum and 0.1% Triton X-100, and then incubated with primary antibodies and HRP-conjugated goat anti-rabbit secondary antibody (Sigma-Aldrich). Antigen-antibody complexes were detected with DAB peroxidase substrate kit (Vector Laboratories) according to the manufacturer's protocol. For immunofluorescence of CTNNB1, antigen retrieval was performed by boiling for 20 minutes in citrate buffer, pH 6.0. Sections were blocked with 5% normal donkey serum for 45 minutes at room temperature, followed by primary and secondary antibodies (each for 1 hour; 1:200 in blocking buffer) at room temperature. Sections were counterstained with DAPI and visualized with standard fluorescence microscopy. The primary antibodies used were anti-CTNNB1 (sc-7199; Santa Cruz Biotechnology Inc.), anti–Ki-67 (Neomarker), and rabbit polyclonal phospho–RPS6 (Ser235/236) antibody (2211; Cell Signaling Technology). For immunofluorescence of ERBB3 and CDH1, 4-μm paraffin sections were baked at 60°C for 30 minutes and then cooled to ambient temperature. Sections were sequentially incubated in xylene (5 minutes twice), 100% ethyl alcohol (5 minutes twice), 95% ethyl alcohol (5 minutes twice), and 80% ethyl alcohol (5 minutes). After washing with water, the sections were antigen retrieved using citrate buffer (pH 6.0; Dako) in a steamer for 25 minutes and cooled 20 minutes at room temperature. Sections were washed with TBS Tween-2 (TBS-T; 10 mM Tris-HCl [pH 7.4], 150 mM NaCl, 0.05% Tween-20), quenched with 3% hydrogen peroxide in TBS for 10 minutes, blocked for avidin/biotin reactivity (00-4303; Zymed, Invitrogen), and blocked with serum-free protein blocking reagent (Invitrogen) for 1 hour at room temperature. Subsequently, the slides were incubated with anti-ERBB3 (sc-285) and anti-CDH1 (sc-7870; both Santa Cruz Biotechnology Inc.) antibodies at 4°C overnight. The immunofluorescence was developed using TSA kits 25 and 22 (Invitrogen) based on the manufacturer's instructions. Adjacent slides were stained with DAPI to visualize nuclei.

Western blot analysis. The jejunum and colon were dissected from 3-month-old mice, cut longitudinally, and washed thoroughly with cold PBS to remove fecal material before being splayed flat on Parafilm. The epithelial layer was harvested by gently scraping the surface with a razor blade, frozen in liquid nitrogen, and stored at –80°C. For collection of tumors, each tumor was microdissected with sharp forceps under a dissecting microscope, frozen in liquid nitrogen, and stored at –80°C. An extract of harvested tissues was prepared by homogenization in buffer (20 mM HEPES [pH 7.4], 150 mM NaCl, 2 mM EDTA, 2 mM EGTA, 0.1% Triton X-100, 10% glycerol, 1 mM phenylmethylsulfonyl fluoride, 1 μg/ml leupeptin, 1 μg/ml aprotinin). The concentration of cleared lysate was measured by the Bradford assay (Bio-Rad), and 14 μg (epithelial scraping) or 2 μg (microadenomas) of protein lysate was loaded onto a 6%–14% acrylamide gel depending on target protein, electrophoresed, and transferred to a PVDF membrane (Bio-Rad). The membrane was incubated in blocking solution containing 5% nonfat dried milk or 1% BSA in TBS-T for 1 hour at room temperature and subsequently incubated with primary antibody in TBS-T at 4°C overnight. After incubation with primary antibody, the membrane was washed 4 times in TBS-T and then incubated in blocking solution containing goat anti-rabbit immunoglobulin conjugated with HRP for 1 hour at room temperature. The membrane was further washed 4 times in TBS-T, and specific protein complexes were visualized with the ECL system or ECL Plus (GE Healthcare). The antibodies used were: EGFR (Maine Biotechnology Services or Lab Vision); ERBB2, ERBB3, ERBB4 (Santa Cruz Biotechnology Inc.); MAPK1/MAPK3, phospho-MAPK1/

MAPK3 (Cell Signaling Technology); AKT, phospho-AKT (Ser473; Cell Signaling Technology); CASP3 (Cell Signaling Technology); PARP (Cell Signaling Technology); phospho-PDK1 (Ser241; BD Biosciences); RPS6, phospho-RPS6 (Ser235/236; Cell Signaling Technology); ACTB (Sigma-Aldrich). Relative intensities of each signal were quantified by scanning X-ray films using LAS 3000 (Fujifilm) and performing densitometry.

Cell culture and siRNA transfection. HCT116 colon cancer cells were maintained in McCoy's 5A medium supplemented with 10% FBS (Invitrogen) at 37°C in a humidified atmosphere of 5% CO$_2$. One day before transfection, 5×10^3 cells were passed to 96-well plates, 1×10^5 cells onto coverslips in 35-mm dishes, or 2×10^5 cells to 6-well plates, and 20 nM of a Stealth siRNA duplex oligonucleotide (Invitrogen) was delivered into cells using Lipofectamine RNAiMAX reagent (Invitrogen). The sense sequences for siRNA duplex were ERBB3-siRNA1, 5′-GGCCAUGAAUGAAUUCUCUA-CUCUA-3′; ERBB3-siRNA3, 5′-CAAUACCAGACACUGUACAAGCUCU-3′; ERBB4-siRNA1, 5′-GAAAUCAGCGCAGGAAACAUCUAUA-3′; and ERBB4-siRNA2, 5′-CCAUCCAGCUGGUUACUCAACUUAU-3′. Two negative controls were used that consisted of transfection reagent only or scrambled duplex with average GC content (Invitrogen). The medium was changed at 1 and 3 days after transfection for cell proliferation assays or 1 day after transfection for TUNEL assays and cell harvesting.

Cell proliferation and TUNEL assays and preparation of cell extracts. Four days after siRNA transfection, cell proliferation was quantified using a colorimetric assay based on the cleavage of the tetrazolium salt WST-1 by mitochondrial dehydrogenases in viable cells (Daeillab). Ninety-six-well plates were incubated at 37°C for 1 hour, and the absorbance was determined at 450 nm on a plate reader (Molecular Devices). Apoptotic cells were quantified with the ApopTag fluorescein in situ apoptosis detection kit (Chemicon, Millipore) according to the manufacturer's protocol and counterstained with DAPI. Cell extracts were prepared by scraping the cells of 6-well plates with homogenation buffer as described above for the mouse tissues.

Statistics. Unpaired Student's *t* test was used to analyze histological scores and densitometry measurements. DSS-induced body weight loss was analyzed by using the Mann-Whitney *U* test. The nonparametric Wilcoxon rank-sum test was used to analyze tumor counts and Student's *t* test for the number of Ki-67– and TUNEL-positive cells. Statistical analysis was performed with StatView (SAS Institute). One-sided *P* values are given, and values less than 0.05 were considered significant.

Address correspondence to: David Threadgill, Department of Genetics, CB#7614, North Carolina State University, Raleigh, North Carolina 27695, USA. Phone: (919) 515-2292; Fax: (919) 515-3355; E-mail: threadgill@ncsu.edu. Or to: Daekee Lee, Science Building C-408, Division of Life and Pharmaceutical Sciences, Ewha Womans University, Seoul 120-720, Republic of Korea. Phone: 82-2-3277-4368; Fax: 82-2-3277-3760; E-mail: daekee@ewha.ac.kr.

1. Hynes, N.E., and Lane, H.A. 2005. ERBB receptors and cancer: the complexity of targeted inhibitors. *Nat. Rev. Cancer.* **5**:341–354.

2. Herbst, R.S., and Sandler, A.B. 2004. Overview of the current status of human epidermal growth factor receptor inhibitors in lung cancer. *Clin. Lung Cancer.* **6**(Suppl. 1):S7–S19.

3. Saltz, L.B. 2004. Palliative management of rectal cancer: the roles of chemotherapy and radiation therapy. *J. Gastrointest. Surg.* **8**:274–276.

4. Rothenberg, M.L., et al. 2005. Randomized phase II trial of the clinical and biological effects of two dose levels of gefitinib in patients with recurrent colorectal adenocarcinoma. *J. Clin. Oncol.* **23**:9265–9274.

5. Cunningham, M.P., Thomas, H., Fan, Z., and Modjtahedi, H. 2006. Responses of human colorectal tumor cells to treatment with the anti-epidermal growth factor receptor monoclonal antibody ICR62 used alone and in combination with the EGFR tyrosine kinase inhibitor gefitinib. *Cancer Res.* **66**:7708–7715.

6. Ponz-Sarvise, M., et al. 2007. Epidermal growth factor receptor inhibitors in colorectal cancer treatment: what's new? *World J. Gastroenterol.* **13**:5877–5887.

7. Fields, A.L.A., et al. 2005. An open-label multicenter phase II study of oral lapatinib (GW572016) as single agent, second-line therapy in patients with metastatic colorectal cancer [abstract]. In *2005 ASCO Annual Meeting Proceedings.* Vol. 23, No. 16S (June 1 Supplement). *J. Clin. Oncol.* **23**:3583.

8. Yarden, Y., and Sliwkowski, M.X. 2001. Untangling the ErbB signalling network. *Nat. Rev. Mol. Cell Biol.* **2**:127–137.

9. Guy, P.M., Platko, J.V., Cantley, L.C., Cerione, R.A., and Carraway, K.L., 3rd. 1994. Insect cell-expressed p180erbB3 possesses an impaired tyrosine kinase activity. *Proc. Natl. Acad. Sci. U. S. A.* **91**:8132–8136.

10. Sierke, S.L., Cheng, K., Kim, H.H., and Koland, J.G. 1997. Biochemical characterization of the protein tyrosine kinase homology domain of the ErbB3 (HER3) receptor protein. *Biochem. J.* **322**:757–763.

11. Soltoff, S.P., Carraway, K.L., 3rd, Prigent, S.A., Gullick, W.G., and Cantley, L.C. 1994. ErbB3 is involved in activation of phosphatidylinositol 3-kinase by epidermal growth factor. *Mol. Cell. Biol.* **14**:3550–3558.

12. Kim, H.H., Sierke, S.L., and Koland, J.G. 1994. Epidermal growth factor-dependent association of phosphatidylinositol 3-kinase with the erbB3 gene product. *J. Biol. Chem.* **269**:24747–24755.

13. Hennessy, B.T., Smith, D.L., Ram, P.T., Lu, Y., and Mills, G.B. 2005. Exploiting the PI3K/AKT pathway for cancer drug discovery. *Nat. Rev. Drug Discov.* **4**:988–1004.

14. Naidu, R., Yadav, M., Nair, S., and Kutty, M.K. 1998. Expression of c-erbB3 protein in primary breast carcinomas. *Br. J. Cancer.* **78**:1385–1390.

15. Ciardiello, F., et al. 1991. Differential expression of epidermal growth factor-related proteins in human colorectal tumors. *Proc. Natl. Acad. Sci. U. S. A.* **88**:7792–7796.

16. Maurer, C.A., et al. 1998. Increased expression of erbB3 in colorectal cancer is associated with concomitant increase in the level of erbB2. *Hum. Pathol.* **29**:771–777.

17. Kobayashi, M., Iwamatsu, A., Shinohara-Kanda, A., Ihara, S., and Fukui, Y. 2003. Activation of ErbB3-PI3-kinase pathway is correlated with malignant phenotypes of adenocarcinomas. *Oncogene.* **22**:1294–1301.

18. Rajkumar, T., Stamp, G.W., Hughes, C.M., and Gullick, W.J. 1996. c-erbB3 protein expression in ovarian cancer. *Clin. Mol. Pathol.* **49**:M199–M202.

19. Friess, H., Guo, X.Z., Nan, B.C., Kleeff, O., and Buchler, M.W. 1999. Growth factors and cytokines in pancreatic carcinogenesis. *Ann. N. Y. Acad. Sci.* **880**:110–121.

20. Holbro, T., et al. 2003. The ErbB2/ErbB3 heterodimer functions as an oncogenic unit: ErbB2 requires ErbB3 to drive breast tumor cell proliferation. *Proc. Natl. Acad. Sci. U. S. A.* **100**:8933–8938.

21. Siegel, P.M., Ryan, E.D., Cardiff, R.D., and Muller, W.J. 1999. Elevated expression of activated forms of Neu/ErbB-2 and ErbB-3 are involved in the induction of mammary tumors in transgenic mice: implications for human breast cancer. *EMBO J.* **18**:2149–2164.

22. Engelman, J.A., et al. 2005. ErbB-3 mediates phosphoinositide 3-kinase activity in gefitinib-sensitive non-small cell lung cancer cell lines. *Proc. Natl. Acad. Sci. U. S. A.* **102**:3788–3793.

23. Engelman, J.A., et al. 2007. MET amplification leads to gefitinib resistance in lung cancer by activating ERBB3 signaling. *Science.* **316**:1039–1043.

24. Erickson, S.L., et al. 1997. ErbB3 is required for normal cerebellar and cardiac development: a comparison with ErbB2-and heregulin-deficient mice. *Development.* **124**:4999–5011.

25. Riethmacher, D., et al. 1997. Severe neuropathies in mice with targeted mutations in the ErbB3 receptor. *Nature.* **389**:725–730.

26. Wu, L., et al. 2003. Extra-embryonic function of Rb is essential for embryonic development and viability. *Nature.* **421**:942–947.

27. Hayashi, S., Lewis, P., Pevny, L., and McMahon, A.P. 2002. Efficient gene modulation in mouse epiblast using a Sox2Cre transgenic mouse strain. *Mech. Dev.* **119**:S97–S101.

28. Madison, B.B., et al. 2002. Cis elements of the villin gene control expression in restricted domains of the vertical (crypt) and horizontal (duodenum, cecum) axes of the intestine. *J. Biol. Chem.* **277**:33275–33283.

29. Hellyer, N.J., Cheng, K., and Koland, J.G. 1998. ErbB3 (HER3) interaction with the p85 regulatory subunit of phosphoinositide 3-kinase. *Biochem. J.* **333**:757–763.

30. Prigent, S.A., and Gullick, W.J. 1994. Identification of c-erbB-3 binding sites for phosphatidylinositol 3′-kinase and SHC using an EGF receptor/c-erbB-3 chimera. *EMBO J.* **13**:2831–2841.

31. Cantley, L.C. 2002. The phosphoinositide 3-kinase pathway. *Science.* **296**:1655–1657.

32. Chen, T., et al. 2003. Regulation of caspase expression and apoptosis by adenomatous polyposis coli. *Cancer Res.* **63**:4368–4374.

33. Roberts, R.B., et al. 2002. Importance of epidermal growth factor receptor signaling in establishment of adenomas and maintenance of carcinomas during intestinal tumorigenesis. *Proc. Natl. Acad. Sci. U. S. A.* **99**:1521–1526.

34. Boudeau, J., Miranda-Saavedra, D., Barton, G.J., and Alessi, D.R. 2006. Emerging roles of pseudokinases. *Trends Cell Biol.* **16**:443–452.

35. Xue, C., et al. 2006. Epidermal growth factor receptor overexpression results in increased tumor cell motility in vivo coordinately with enhanced intravasation and metastasis. *Cancer Res.* **66**:192–197.

36. Lee, D., et al. 2004. Wa5 is a novel ENU-induced antimorphic allele of the epidermal growth factor receptor. *Mamm. Genome.* **15**:525–536.

37. Schmelz, E.M., et al. 2007. Regression of early and intermediate stages of colon cancer by targeting multiple members of the EGFR family with EGFR-related protein. *Cancer Res.* **67**:5389–5396.

38. Asnaghi, L., et al. 2004. Bcl-2 phosphorylation and apoptosis activated by damaged microtubules require mTOR and are regulated by Akt. *Oncogene.* **23**:5781–5791.

39. Dignass, A.U., and Sturm, A. 2001. Peptide growth factors in the intestine. *Eur. J. Gastroenterol. Hepatol.* **13**:763–770.

40. Moran, A.E., et al. 2004. Apc deficiency is associated with increased Egfr activity in the intestinal enterocytes and adenomas of C57BL/6J-Min/+ mice. *J. Biol. Chem.* **279**:43261–43272.

41. Schwartz, F., et al. 1991. A dominant positive and negative selectable gene for use in mammalian cells. *Proc. Natl. Acad. Sci. U. S. A.* **88**:10416–10420.

42. Nagy, A., Gertsenstein, M., Vintersten, K., and Behringer, B. 2003. *Manipulating the mouse embryo: a laboratory manual.* Cold Spring Harbor Laboratory Press. Cold Spring Harbor, New York, USA. 800 pp.

43. Lee, D., et al. 2004. Epiregulin is not essential for development of intestinal tumors but is required for protection from intestinal damage. *Mol. Cell. Biol.* **24**:8907–8916.

44. Kaiser, S., et al. 2007. Transcriptional recapitulation and subversion of embryonic colon development by mouse colon tumor models and human colon cancer. *Genome Biol.* **8**:R131.